Sustainable Energy & Fuels

ROYAL SOCIETY OF CHEMISTRY

PAPER

View Article Online
View Journal | View Issue

Cite this: *Sustainable Energy Fuels*, 2022, **6**, 894

Visible light-initiated aerobic oxidation of amines to imines over TiO_2 microspheres with $TEMPO^+PF_6^-$†

Jun Zhou, Xiaoming Ma, Yuexin Wang, Xia Li and Xianjun Lang *

Semiconductor photocatalysis holds great promise to drive vital chemical reactions utilizing sunlight. Amongst semiconductors, TiO_2-related materials are one of the most viable to achieve enhanced photocatalytic performances because of their intrinsic merits. Here TiO_2 microspheres assembled from nanocrystals with a distinct hierarchical architecture and a high specific surface area were fabricated using a simple template-free solvothermal process. Assembling amines on TiO_2 microspheres initiated by visible light can lead to a surface complex that captures visible light for further oxidation of amines. Moreover, the selective oxidation of amines could be boosted by fully exploring the surface polarity of TiO_2 microspheres with more polar 2,2,6,6-tetramethylpiperidine-1-oxoammonium hexafluorophosphate ($TEMPO^+PF_6^-$) instead of (2,2,6,6-tetramethylpiperidin-1-yl)oxyl (TEMPO) as the redox mediator. As such, cooperative photocatalysis with $TEMPO^+PF_6^-$ was framed over TiO_2 microspheres to initiate the efficient and selective aerobic oxidation of benzyl amines into imines. Significantly, the activity of $TEMPO^+PF_6^-$ surpassed that of TEMPO in aiding the visible light-initiated selective oxidation of amines over TiO_2 microspheres, reaching more than about 3 times in some cases. This work suggests that the surface properties of a semiconductor could be maneuvered to enable coupling with a suitable redox mediator to ameliorate selective organic conversions in an unprecedented manner.

Received 17th November 2021
Accepted 31st December 2021

DOI: 10.1039/d1se01829a

rsc.li/sustainable-energy

1. Introduction

Selective organic conversions using solar energy to manufacture value-added products could potentially become prominent in sustainable synthesis.[1–7] In the past few decades, semiconductor photocatalysis has matured by virtue of its prowess to build sustainable chemical avenues under mild conditions.[8–14] Owing to its intrinsic merits, photochemical stability, and environmental benignity, TiO_2 has been one of the most prevalent photocatalysts since its inception.[15–19] However, developing new TiO_2-related materials is ponderable for enhanced photocatalytic performance.[20–25] Self-assembly of TiO_2 nanocrystals into porous microspheres merits special attention on account of their fascinating optical properties and ease of recycling in practical applications.[26–28] Specifically, the porous nature and high specific surface areas of TiO_2 microspheres are favorable for increasing the density of active sites with good approachability and the diffusion of substrates and products.[29,30] Furthermore, their unique structures feature boosted light-harvesting capabilities through absorbing light as much as possible and enhancing light scattering.[31] Nevertheless, the wide optical bandgap is detrimental to the photocatalytic performance of TiO_2 microspheres, which has severely hindered the exploitation of solar energy and thereby their quantum efficiencies for photocatalytic reactions.[32–34]

So far, much effort has been exerted to explore diverse modification strategies for TiO_2 to eliminate the encountered obstacles aiming at utilizing a broader solar spectrum.[35–37] In this regard, surface modification of TiO_2 with organic ligands has been spotlighted to develop visible light-responsive complex by ligand-to-metal charge transfer.[38,39] Along these lines, it is intriguing that amines as N-containing molecules can directly be assembled onto the surface of TiO_2, affording a surface complex that captures visible light to further initiate the oxidation of amines into imines.[40,41] Importantly, imines are vital in constructing fine chemicals and various *N*-heterocyclic compounds with pharmacological activities.[42–47] This phenomenon not only reduces the utilization of organic ligands but also contributes to further excavating reaction mechanisms. However, the actual photocatalytic efficiency of TiO_2 for selective aerobic oxidation of amines to imines is not satisfactory due to the low electron transfer efficiency.

To address this issue, choosing a superior redox mediator is necessary, facilitating electron transfer among amines, O_2, and TiO_2. Numerous robust systems of cooperative photocatalysis have been devised with the assistance of the stable nitroxyl

Sauvage Center for Molecular Sciences and Hubei Key Lab on Organic and Polymeric Optoelectronic Materials, College of Chemistry and Molecular Sciences, Wuhan University, Wuhan 430072, China. E-mail: xianjunlang@whu.edu.cn

† Electronic supplementary information (ESI) available. See DOI: 10.1039/d1se01829a

radical TEMPO because of its excellent redox behavior.[48–51] To our knowledge, the photocatalytic efficiency could be ameliorated by replacing TEMPO with its more polar oxoammonium salt as the redox mediator under certain conditions.[52] In this regard, $TEMPO^+PF_6^-$ might be a preferential candidate to fully explore the surface polarity of TiO_2 microspheres, hence boosting the selective oxidation of amines.

Herein, TiO_2 microspheres assembled from nanocrystals were fabricated through a simple one-pot, template-free solvothermal process.[26] The high specific surface area, porous nature, and distinct hierarchical architecture make TiO_2 microspheres a prominent candidate for photocatalytic selective oxidation of amines in air. Several typical amines can be adsorbed onto the surface of TiO_2 microspheres to provide a visible light-responsive surface complex. A well-designed paradigm of cooperative photocatalysis with $TEMPO^+PF_6^-$ was framed over TiO_2 microspheres for the blue light-initiated efficient and selective oxidation of benzyl amines to imines in air. As a redox mediator, the activity of $TEMPO^+PF_6^-$ surpassed that of TEMPO in aiding the visible light-initiated selective oxidation of amines over TiO_2 microspheres, reaching more than about 3 times in some cases. This work suggests that the surface properties of a semiconductor could be maneuvered to couple with a suitable redox mediator to ameliorate selective organic conversions in an unprecedented manner.

2. Results and discussion

2.1 Materials characterizations of TiO_2 microspheres

The morphology and microstructure of the TiO_2 sample have been determined by field emission scanning electron microscopy (FESEM) and transmission electron microscopy (TEM). It can be seen from the FESEM image (Fig. 1a) that most of the TiO_2 sample are spherical with nearly the same size, though some of them aggregate together. As shown in Fig. 1b, the TiO_2 microspheres made up of interconnected nanocrystals are highly porous, and their diameters are about 1.4 μm. The TEM images (Fig. 1c and d) further prove the porous nature of TiO_2 microspheres. The large spherical geometry and highly porous nanostructure result in a lighter contrast along the TiO_2 microspheres' edge in comparison with the dark center. The high-resolution TEM (HRTEM) image in Fig. 1e indicates distinct lattice fringes with interplanar spacing of 0.19, 0.23, and 0.35 nm, which are readily indexed to the (2 0 0), (0 0 4), and (1 0 1) planes of tetragonal anatase phase. Furthermore, the tetragonal anatase phase of TiO_2 microspheres has further been confirmed by powder X-ray diffraction (PXRD) characterization (Fig. S1, see the ESI†).

The pore characteristics and Brunauer–Emmett–Teller (BET) specific surface area of the TiO_2 microspheres were analyzed by N_2 sorption measurements. According to the IUPAC classification, a type IV isotherm with an H2 hysteresis loop was observed in the N_2 adsorption–desorption isotherms of the TiO_2 microspheres (Fig. 2a), illustrating the mesoporous nature of the TiO_2 microspheres. It can be well perceived from Barrett–Joyner–Halenda (BJH) analysis (Fig. 2b). The pore size distribution of TiO_2 microspheres is narrow and most of the pores possess an average pore size of 8 nm. Besides, the pore volume of the TiO_2 microspheres is 0.39 $cm^3\ g^{-1}$ and their BET specific surface area is 148.57 $m^2\ g^{-1}$. The large pore volume and high specific surface area of TiO_2 microspheres are favorable for furnishing

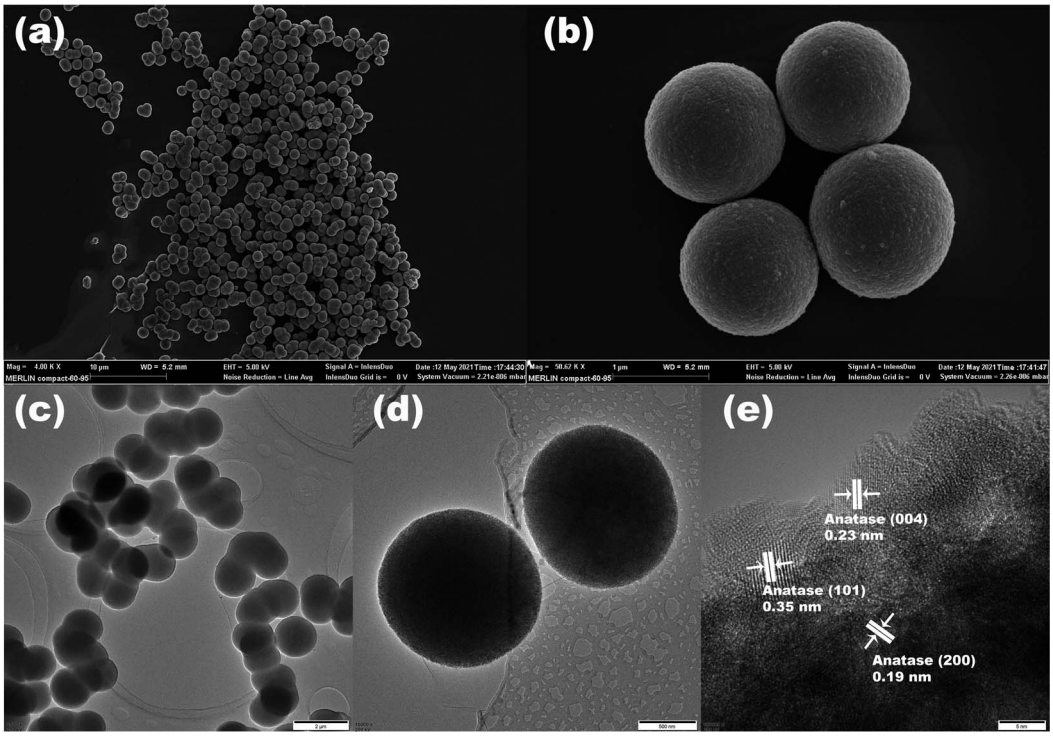

Fig. 1 FESEM images (a and b), TEM images (c and d), and HRTEM image (e) of the TiO_2 microspheres.

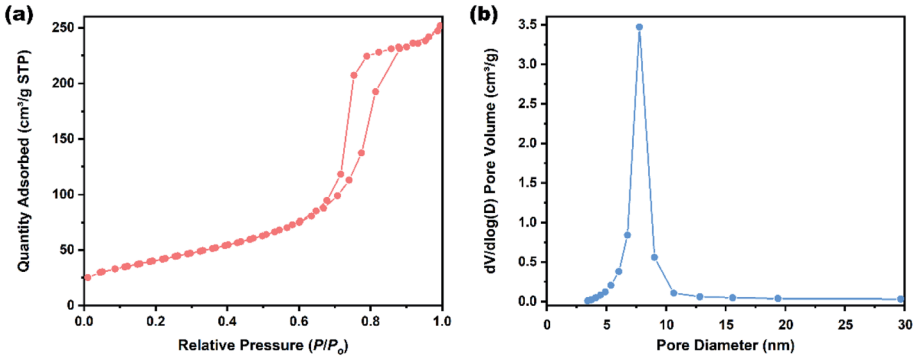

Fig. 2 (a) N_2 adsorption and desorption isotherms and (b) pore size distribution (BJH desorption) plot of the TiO_2 microspheres.

more active sites and facilitating mass and charge transport. Likewise, the surface hydroxyl groups could dictate the surface polarity, the adsorption capacity, and the photocatalytic efficiency of TiO_2 microspheres.[53] Thus, the surface hydroxyl group density of TiO_2 microspheres was measured to be 7.40 nm^{-2} by thermogravimetric analysis (TGA) based on a reported protocol (Fig. S2†),[54] much higher than that reported for Aeroxide P25 TiO_2 (5.30 nm^{-2}).[55] And the concentration of the surface hydroxyl group of TiO_2 microspheres was also calculated to be 1.83 mmol g^{-1} by considering the specific surface area, which is higher than 0.47 mmol g^{-1} in the case of Aeroxide P25 TiO_2.[55] Taking all of these into account, TiO_2 microspheres might be an attractive photocatalytic material.

However, upgrading the photocatalytic performance of TiO_2 microspheres appears to be a necessity because of the poor visible light absorption caused by the wide bandgap. During the processes of converting amines into imines, it can be distinctly noticed that the original white TiO_2 sample turned yellowish without any other added ligand after a short induction period. This phenomenon reveals that amines, as N-containing molecules, can be assembled onto the surface of TiO_2 to form a complex. The formed surface complex was further investigated by X-ray photoelectron spectroscopy (XPS) analysis (Fig. 3a and S3†). The N 1s high-resolution XPS in Fig. 3a depicts two binding energy peaks at 400.2 eV and 399.2 eV ascribed to the N–C bond and N–Ti–O, respectively. This proves that benzylamine was successfully assembled on the surface of TiO_2 microspheres by the interaction between N and Ti. Next, the visible light harvesting ability of the assembled surface complex was assessed by UV-vis diffuse reflectance spectroscopy (DRS). As shown in Fig. 3b, the light absorption edge of benzylamine–TiO_2 microspheres generates a significant bathochromic shift compared with that of pure TiO_2 microspheres, which partly tallies with the light-emitting spectrum of blue light-emitting diodes (LEDs). Next, the photocatalytic performance of TiO_2 microspheres was checked by the visible light-initiated selective aerobic oxidation of benzylamine. According to the control experiments exposed to different LEDs (Fig. S4†), blue and purple LEDs were all valid ones. But considering the background purple light absorption of TiO_2 microspheres, blue LEDs are the more suitable ones for further investigations.

2.2 Selective photocatalytic oxidation of amine over TiO_2 microspheres with $TEMPO^+PF_6^-$

To gain some insights, a sequence of kinetic studies were performed for the selective aerobic oxidation of benzylamine under different conditions (Fig. 4a). No detectable conversion of benzylamine was observed without photocatalyst's involvement. When only TiO_2 microspheres were applied as the photocatalyst, only minor conversion of benzylamine was observed. With advent of TEMPO, the photocatalytic conversion of

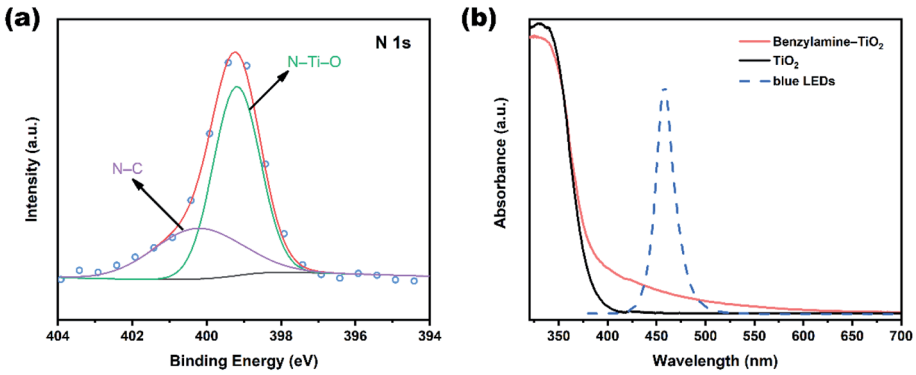

Fig. 3 (a) High-resolution XPS spectrum of N 1s; (b) UV-vis DRS spectra of the TiO_2 microspheres and benzylamine–TiO_2 microspheres, and light-emitting spectrum of blue LED.

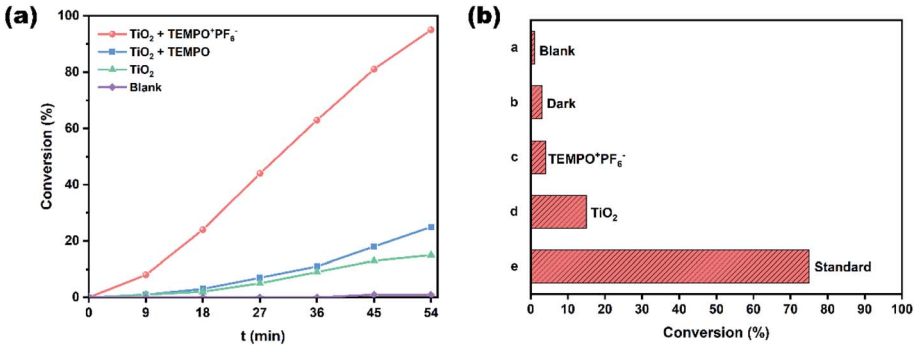

Fig. 4 (a) Kinetic plots for the blue light-initiated selective aerobic oxidation of benzylamine under different conditions; (b) control experiments for the blue light-initiated selective aerobic oxidation of benzylamine over TiO_2 microspheres with $TEMPO^+PF_6^-$. (a), blank; (b), dark; (c), $TEMPO^+PF_6^-$ only; (d), TiO_2 microspheres only; (e), standard. Standard conditions: benzylamine (0.5 mmol), air (1 atm), TiO_2 microspheres (40 mg), $TEMPO^+PF_6^-$ (0.015 mmol), CH_3CN (1 mL), blue LEDs (460 ± 10 nm), 0.7 h.

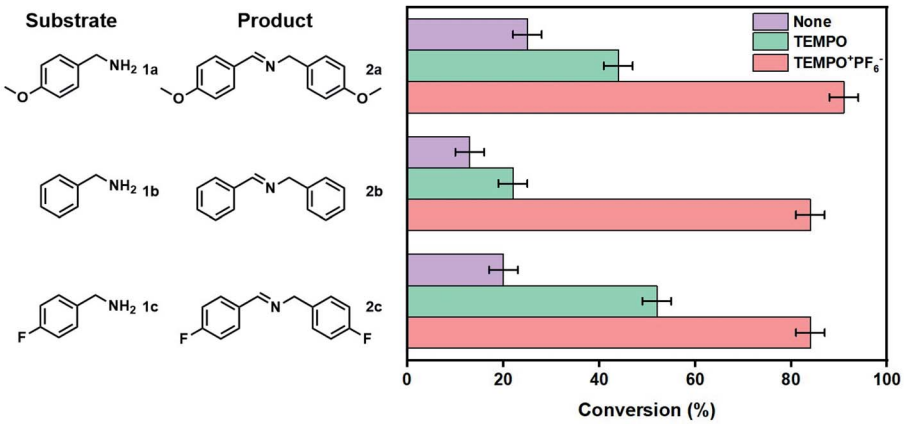

Fig. 5 Comparative experiments for the blue light-initiated selective aerobic oxidation of different amines into imines over TiO_2 microspheres with different redox mediators. Reaction conditions: amine (0.5 mmol), air (1 atm), TiO_2 microspheres (40 mg), TEMPO or $TEMPO^+PF_6^-$ (0.015 mmol), CH_3CN (1 mL), blue LEDs (460 ± 10 nm), 0.8 h.

benzylamine improved apparently. Of note, once TEMPO was superseded by $TEMPO^+PF_6^-$, a significantly enhanced photocatalytic conversion was observed. The enhancement is mainly due to the higher polarity of $TEMPO^+PF_6^-$ than TEMPO. When $TEMPO^+PF_6^-$ was added into the reaction system, the conversion of benzylamine increased by 5 times compared with that of pure TiO_2 microspheres and by nearly 2.8 times compared with that of synergic TiO_2 microspheres and TEMPO. This meliority

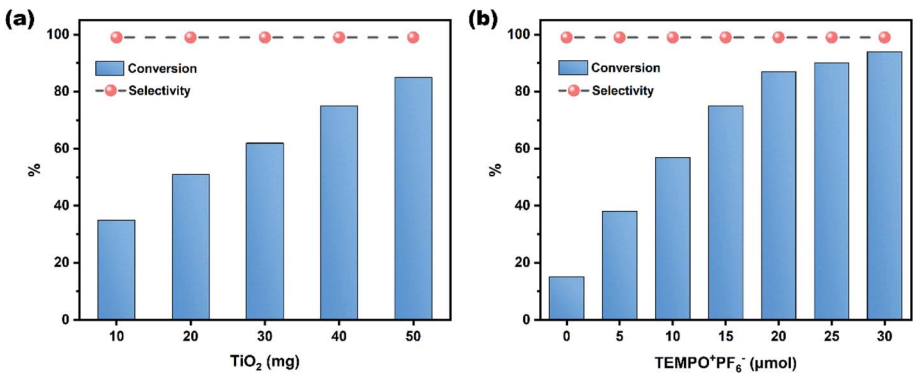

Fig. 6 (a) The influence of the amounts of TiO_2 microspheres on the blue light-initiated selective oxidation of benzylamine. Reaction conditions: benzylamine (0.5 mmol), air (1 atm), $TEMPO^+PF_6^-$ (0.015 mmol), CH_3CN (1 mL), blue LEDs (460 ± 10 nm), 0.7 h. (b) The influence of the amounts of $TEMPO^+PF_6^-$ on the blue light-initiated selective oxidation of benzylamine. Reaction conditions: benzylamine (0.5 mmol), air (1 atm), TiO_2 microspheres (40 mg), CH_3CN (1 mL), blue LEDs (460 ± 10 nm), 0.7 h.

holds for other typical benzyl amines as well (Fig. 5). Moreover, all the photocatalytic systems mentioned above have an induction period of about 9 minutes. It was speculated that a new visible light absorption band was generated due to the blue light-initiated interaction of benzylamine and TiO_2 microspheres. After the induction period, all reactions followed zero-order kinetics. In addition, the reaction kinetic isotope effect (KIE) was also investigated by replacing benzylamine with benzyl-α,α-d_2-amine (Fig. S5†). Likewise, the selective aerobic oxidation of benzyl-α,α-d_2-amine obeyed zero-order kinetics, thereby the reaction proceeding at a slower rate. This phenomenon implies that C_α–H breakage can profoundly impact the photocatalytic rate. The control experiments in Fig. 4b demonstrate that the system can only be efficient when all constituents such as blue LEDs, TiO_2 microspheres, and $TEMPO^+PF_6^-$ work together.

Except for the bandgap, the crystal phase, microstructure, and specific surface area also determine the efficiency of a photocatalyst. Therefore, it is also crucial to identify a suitable photocatalyst. Three other different types of TiO_2 were then selected as photocatalysts to cooperate with $TEMPO^+PF_6^-$ to conduct the blue light-initiated selective aerobic oxidation of benzylamine. As shown in Table S1,† all the types of TiO_2 were applicable to this system. However, the TiO_2 microspheres turned out to be the best ones attributed to their large pore volume and high specific surface area, just as assumed.

Table 1 Blue light-initiated selective aerobic oxidation of amines to imines over TiO_2 microspheres with $TEMPO^+PF_6^{-a}$

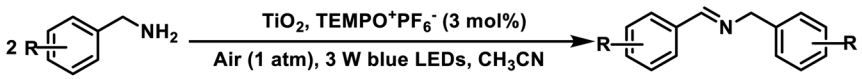

Entry	Substrate	Product	t (h)	Conv.[b] (%)	Sel.[b] (%)
1		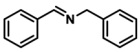	0.9	92	99
2		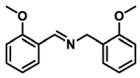	0.9	96	99
3	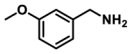	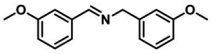	1.1	97	99
4	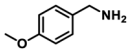	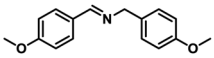	0.8	91	99
5	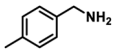	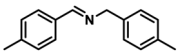	0.9	96	99
6	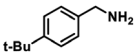	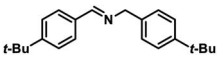	2.5	82	99
7	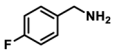	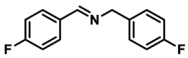	1.0	96	99
8	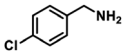	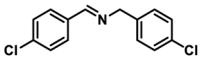	1.2	95	99
9	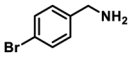	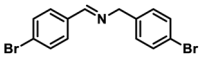	1.2	96	99
10	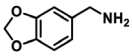	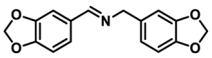	1.1	93	99
11		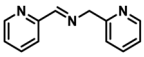	1.2	91	99
12	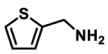	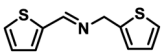	2.0	85	98
13	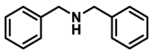	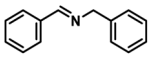	1.0	80	77
14	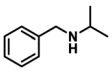	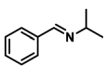	1.0	65	63

[a] Reaction conditions: amine (0.5 mmol for entries 1–12; 0.25 mmol for entries 13 and 14) , air (1 atm), TiO_2 microspheres (40 mg), $TEMPO^+PF_6^-$ (0.015 mmol), CH_3CN (1 mL), blue LEDs (460 ± 10 nm). [b] Determined by GC–FID using chlorobenzene as the internal standard, conversion of amines, and selectivity of the corresponding imines.

Furthermore, a mixed oxide TiO_2/SiO_2 (1 : 1) was also tested as a photocatalyst. However, only a slight conversion of benzylamine was observed (Table S1,† entry 5).

Considering the indispensability of TiO_2 microspheres in the meticulously designed photocatalytic system, the effect of the amounts of TiO_2 microspheres was examined on the blue light-initiated selective aerobic oxidation of benzylamine. As depicted in Fig. 6a, the gradually increased conversions are perceived with the increased amounts of TiO_2 microspheres, implying that more O_2 has been activated on the conduction band of TiO_2 microspheres. Furthermore, $TEMPO^+PF_6^-$ as a redox mediator could ensure electron transfer between benzylamine, O_2, and TiO_2 microspheres. The effect of $TEMPO^+PF_6^-$ was thus thoroughly explored (Fig. 6b). As the amount of $TEMPO^+PF_6^-$ increases, the conversion gradually accelerates, but finally tends to plateau. This phenomenon means that there is a potential saturation point.

Besides, the influence of solvents was thoroughly tested (Table S2†). CH_3CN is the best one with the highest conversion of benzylamine and high selectivity. A non-polar solvent, cyclohexane, is also applicable but with some drop in conversion of benzylamine. However, when the photocatalytic reaction was carried out in protic solvents like C_2H_5OH or CH_3OH, both the conversions and selectivities decreased significantly due to redox-active nature of the solvents. Additionally, the cycling stability is of common concern. The reusability of TiO_2 microspheres was thus evaluated for the blue light-initiated selective aerobic oxidation of benzylamine. As disclosed in Fig. S6,† the activity of the reused TiO_2 microspheres showed only a slight decline due to the partial loss during recovery.

To extend the utilization range of this photocatalytic system, the photocatalytic selective aerobic oxidation of various amines under the optimal conditions has been carried out (Table 1). The blue light-initiated selective oxidation of benzylamine and its derivatives proceeded smoothly with high conversions and selectivities of their corresponding imines (Table 1, entries 1–10). The effect of the positions of the substituents on the conversions of the amines was evaluated by oxidizing the *ortho*-, *meta*-, and *para*-substituted methoxyl benzylamines. As seen, *ortho*- and *para*-substituted methoxyl benzylamines can be converted to the desired imine with much higher conversions (Table 1, entries 2–4). In addition, the oxidation of benzylamines with electron-donating substituents shows a more rapid conversion rate compared with that of electron-withdrawing substituents (Table 1, entries 4, 5 and 7–9). Nevertheless, it can be concluded that the photocatalytic oxidation of benzyl amines has great tolerance of the position and the type of substituents. Moreover, piperonylamine and heterocyclic amines can also be transformed into the corresponding imines with high selectivities and feasible conversions (Table 1, entries 10–12), though more time was taken in the case of 2-thiophenemethylamine. Furthermore, secondary amines can also be transformed into imines with comparable conversions (Table 1, entries 13 and 14), though partially influenced by steric hindrance between $TEMPO^+PF_6^-$ and secondary amines.

2.3 Probing the mechanism for the photocatalytic selective oxidation of amines

To detect reactive oxygen species (ROS) in the photocatalytic selective oxidation of benzylamine, the trapping experiments were performed by utilizing different scavengers (Table 2). When the reaction Pyrex vessel was filled with N_2 instead of aerial O_2, the photocatalytic oxidation of benzylamine completely was shut down, implying that O_2 is the sole oxidant (Table 2, entry 1). A significantly declined conversion of benzylamine appeared with *p*-benzoquinone (*p*-BQ) to trap the superoxide anion radical ($O_2^{\bullet-}$) (Table 2, entry 3), testifying to the crucial role of $O_2^{\bullet-}$ in this system. Besides, a similar outcome was obtained when $AgNO_3$, a scavenger for e_{cb}^-, was included (Table 2, entry 2). This was attributed to the formed $O_2^{\bullet-}$ being intercepted by $AgNO_3$. Both isopropyl alcohol (IPA) and CD_3CN solvent, acting as an $^\bullet OH$ scavenger and singlet oxygen ($^1O_2$) maintainer, respectively, had a negligible effect (Table 2, entries 4 and 5).

To gain more insight into the aerobic oxidation of amines to imines, the influence of O_2 pressure and *in situ* electron paramagnetic resonance (EPR) spectra were recorded (Fig. 7). Thus, the influence of O_2 pressure on the blue light-initiated selective aerobic oxidation of benzylamine was monitored (Fig. 7a). The conversion of benzylamine was augmented with the boosted

Table 2 Quenching experiments to determine the ROS for the blue light-initiated selective aerobic oxidation of benzylamine[a]

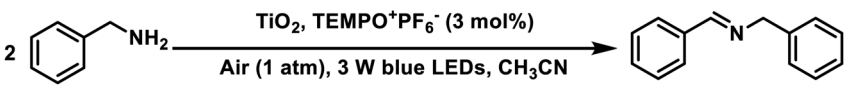

Entry	Quencher (equiv.)	Roles	Conv.[b] (%)
1	N_2 (—)	O_2 replacement	0
2	$AgNO_3$ (1)	e_{cb}^- scavenger	14
3	*p*-BQ (0.2)	$O_2^{\bullet-}$ scavenger	9
4	IPA (2)	$^\bullet OH$ scavenger	70
5	CD_3CN (1 mL)	$^1O_2$ maintainer	75

[a] Reaction conditions: benzylamine (0.5 mmol), air (1 atm), TiO_2 microspheres (40 mg), $TEMPO^+PF_6^-$ (0015 mmol), CH_3CN (1 mL), blue LEDs (460 ± 10 nm), 0.7 h. [b] Determined by GC–FID using chlorobenzene as the internal standard, conversion of benzylamine.

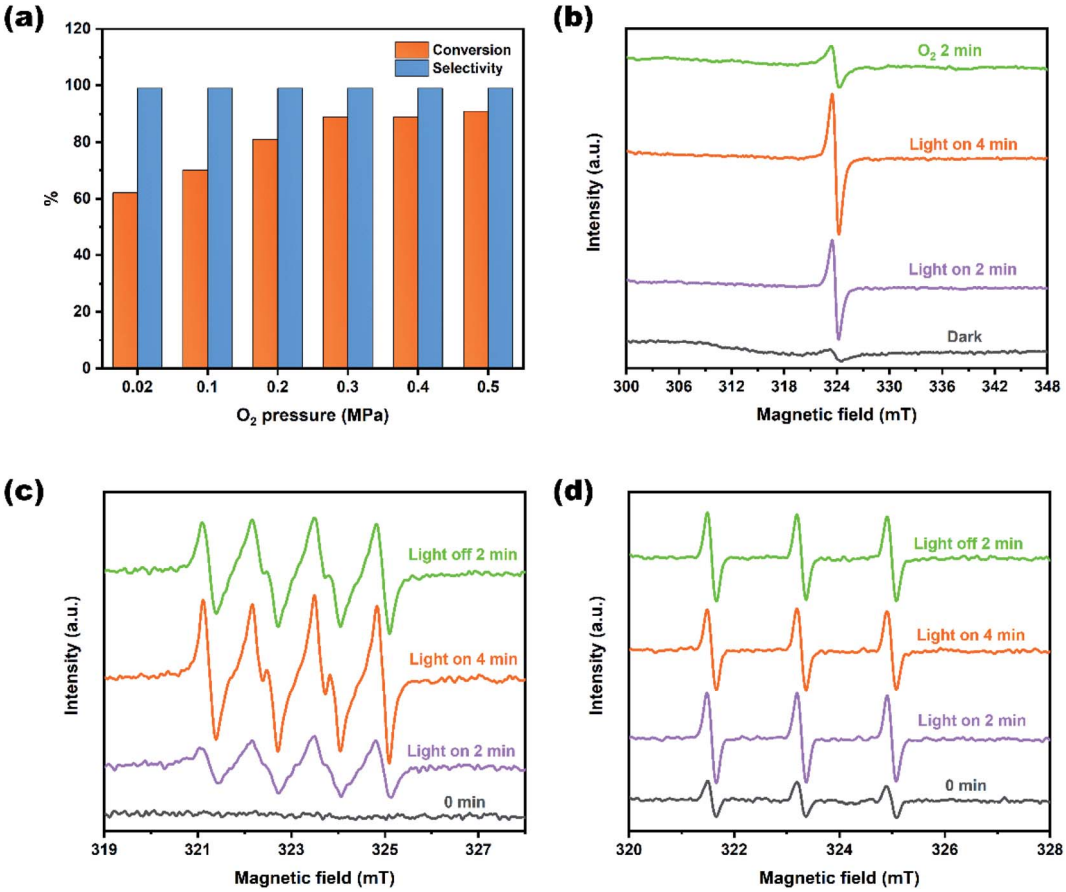

Fig. 7 (a) Influence of the O_2 pressure for the blue light-initiated selective aerobic oxidation of benzylamine over TiO_2 microspheres with $TEMPO^+PF_6^-$. The EPR spectra recorded during the the blue light-initiated selective oxidation of benzylamine: (b) e_{cb}^-, (c) spin trapping of $O_2^{\bullet-}$ with DMPO, and (d) $TEMPOH^+PF_6^-$.

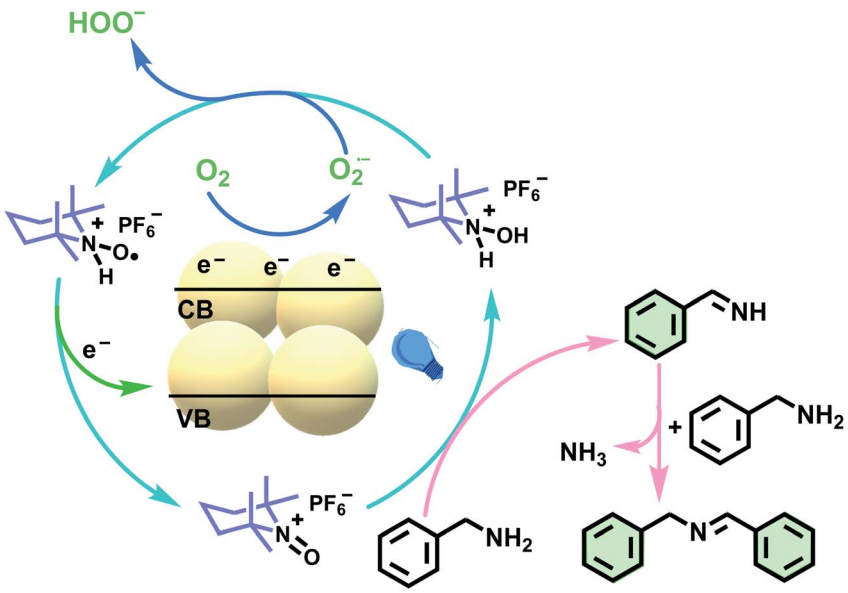

Scheme 1 A plausible mechanism for visible light-initiated aerobic oxidation of benzylamine into imine over TiO_2 microspheres with $TEMPO^+PF_6^-$.

O_2 pressure at an early stage. Nevertheless, once O_2 pressure reached 0.3 MPa, further increasing it did not visibly improve the conversion. Fig. 7b depicts the EPR signal of the conduction band electron (e_{cb}^-) during the oxidation process. A weak signal of e_{cb}^- was observed in the dark due to the inherent oxygen vacancies of TiO_2. Subsequently, the signal for e_{cb}^- strengthens gradually with prolonged exposure time under visible light. However, once O_2 was introduced into the system, the signal for e_{cb}^- noticeably reduces, implying that the e_{cb}^- transferred to O_2. Then, 5,5-dimethyl-1-pyrroline-*N*-oxide (DMPO) was added to trap $O_2^{\bullet-}$. The enhanced signal confirms that $O_2^{\bullet-}$ had participated in the reaction pathway under visible light irradiation (Fig. 7c). Finally, the EPR test of $TEMPOH^+PF_6^-$, the intermediate product of $TEMPO^+PF_6^-$, was also performed, aiming at gaining a deeper understanding of the $TEMPO^+PF_6^-$ redox process. As seen in Fig. 7d, the characteristic signal of $TEMPOH^+PF_6^-$ increases when exposed to blue LEDs, since $TEMPO^+PF_6^-$ transformed into $TEMPOH^+PF_6^-$. However, with prolonged time of exposure, the intensity of $TEMPOH^+PF_6^-$ slightly weakens, attesting to the transformation between $TEMPOH^+PF_6^-$, $TEMPO^+PF_6^-$ and $TEMPOH_2^+PF_6^-$ accordingly. Presumably, the driving force between the redox mediator $TEMPO^+PF_6^-$ in a non-conductive solvent like CH_3CN over TiO_2 microspheres is collisional electron transfer which also occurs in other photocatalytic system.[56]

Referring to the above analysis, a plausible mechanism is proposed for cooperative photocatalysis of TiO_2 microspheres with $TEMPO^+PF_6^-$ in Scheme 1. Exposed to blue LEDs, free benzylamine in the solution can self-assemble onto the surface of TiO_2 microspheres in advance to generate a new visible light absorption band. Then, electrons from the highest occupied molecular orbital (HOMO) of the adsorbate migrate into the conduction band of TiO_2 microspheres, resulting in a radical cation on the surface of benzylamine–TiO_2 complex. Subsequently, aerial O_2 accepts e_{cb}^- to form $O_2^{\bullet-}$. Meanwhile, $TEMPO^+PF_6^-$ can act as a stoichiometric oxidant to directly oxidize benzylamine into benzylideneamine, turning into $TEMPOH_2^+PF_6^-$ itself. The resultant benzylideneamine then couples with benzylamine to supply the desired *N*-benzylidenebenzylamine. Finally, $TEMPOH_2^+PF_6^-$ is oxidized by $O_2^{\bullet-}$ to give $TEMPOH^+PF_6^-$, which can cause the radical cation on the surface of benzylamine–TiO_2 complex to return to its ground state. And $TEMPO^+PF_6^-$ is renewed simultaneously.

3. Conclusions

In summary, TiO_2 microspheres with a distinct hierarchical architecture and a high specific surface area were fabricated by a facile one-pot, template-free solvothermal process. A well-designed paradigm of cooperative photocatalysis with $TEMPO^+PF_6^-$ was framed over TiO_2 microspheres for visible light-initiated efficient and selective oxidation of benzyl amines into imines in air. No extra organic ligand was required since the visible light-initiated assembly of amines on TiO_2 microspheres can lead to a surface complex that captures visible light to further initiate the oxidation of amines. The selective oxidation of amines could be boosted by fully exploring the surface polarity of TiO_2 microspheres with more polar $TEMPO^+PF_6^-$ instead of TEMPO as the redox mediator. Control results confirmed that the activity of $TEMPO^+PF_6^-$ has surpassed that of TEMPO in aiding the visible light-initiated selective oxidation of amines over TiO_2-microspheres, reaching more than about 3 times in some cases. This work suggests that the surface properties of a semiconductor could be maneuvered to enable coupling with a suitable redox mediator to ameliorate selective organic conversions in an unprecedented manner.

Conflicts of interest

There are no conflicts to declare.

Acknowledgements

This work was funded by the National Natural Science Foundation of China (Grants 22072108 and 21773173).

References

1 C. Han, Z. Chen, N. Zhang, J. C. Colmenares and Y. J. Xu, *Adv. Funct. Mater.*, 2015, **25**, 221–229.
2 S. J. Zhang, W. X. Huang, X. L. Fu, X. Z. Zheng, S. G. Meng, X. J. Ye and S. F. Chen, *Appl. Catal., B*, 2018, **233**, 1–10.
3 Y. Q. Xing, Z. R. Tan, J. Z. Cheng, Z. Q. Shen, Y. J. Zhang, L. Chen and S. Y. Liu, *Sustainable Energy Fuels*, 2021, **5**, 5166–5174.
4 J. Ding, W. Xu, H. Wan, D. S. Yuan, C. Chen, L. Wang, G. F. Guan and W. L. Dai, *Appl. Catal., B*, 2018, **221**, 626–634.
5 X. N. Tan, J. L. Zhang, J. B. Shi, X. Y. Cheng, D. X. Tan, B. X. Zhang, L. F. Liu, F. Y. Zhang, B. X. Han and L. R. Zheng, *Sustainable Energy Fuels*, 2020, **4**, 2823–2830.
6 S. Hoang and P. X. Gao, *Adv. Energy Mater.*, 2016, **6**, 1600683.
7 J. Y. Ma, X. J. Tan, Q. Q. Zhang, Y. Wang, J. L. Zhang and L. Z. Wang, *ACS Catal.*, 2021, **11**, 3352–3360.
8 W. J. Ong, L. L. Tan, Y. H. Ng, S. T. Yong and S. P. Chai, *Chem. Rev.*, 2016, **116**, 7159–7329.
9 J. X. Low, J. G. Yu, M. Jaroniec, S. Wageh and A. A. Al-Ghamdi, *Adv. Mater.*, 2017, **29**, 1601694.
10 X. Li, J. G. Yu and M. Jaroniec, *Chem. Soc. Rev.*, 2016, **45**, 2603–2636.
11 H. J. Li, Y. Zhou, W. G. Tu, J. H. Ye and Z. G. Zou, *Adv. Funct. Mater.*, 2015, **25**, 998–1013.
12 Y. X. Fang, X. Z. Fu and X. C. Wang, *ACS Mater. Lett.*, 2020, **2**, 975–980.
13 S. Q. Wu, X. J. Tan, J. Y. Lei, H. J. Chen, L. Z. Wang and J. L. Zhang, *J. Am. Chem. Soc.*, 2019, **141**, 6592–6600.
14 Y. Liu, P. Zhang, B. Z. Tian and J. L. Zhang, *ACS Appl. Mater. Interfaces*, 2015, **7**, 13849–13858.
15 Z. Shayegan, C. S. Lee and F. Haghighat, *Chem. Eng. J.*, 2018, **334**, 2408–2439.
16 H. Khan, M. G. Rigamonti, G. S. Patience and D. C. Boffito, *Appl. Catal., B*, 2018, **226**, 311–323.
17 L. F. Wei, C. L. Yu, Q. H. Zhang, H. Liu and Y. Wang, *J. Mater. Chem. A*, 2018, **6**, 22411–22436.

18 Z. H. Zhao, J. Tian, Y. H. Sang, A. Cabot and H. Liu, *Adv. Mater.*, 2015, **27**, 2557–2582.
19 Y. X. Fang, Y. Zheng, T. Fang, Y. Chen, Y. D. Zhu, Q. Liang, H. Sheng, Z. S. Li, C. C. Chen and X. C. Wang, *Sci. China: Chem.*, 2020, **63**, 149–181.
20 V. Etacheri, C. Di Valentin, J. Schneider, D. Bahnemann and S. C. Pillai, *J. Photochem. Photobiol., C*, 2015, **25**, 1–29.
21 W. Zhang, H. L. He, Y. Tian, H. Z. Li, K. Lan, L. H. Zu, Y. Xia, L. L. Duan, W. Li and D. Y. Zhao, *Nano Energy*, 2019, **66**, 104113.
22 Z. R. Wang, Y. L. Tong, L. Y. Dang, F. Gao and Q. Y. Lu, *Chem. Eng. J.*, 2019, **370**, 1434–1439.
23 J. L. Zhang, H. C. Tao, S. S. Wu, J. L. Yang and M. S. Zhu, *Appl. Catal., B*, 2021, **296**, 120372.
24 Y. Chen, M. J. Xu, J. Y. Wen, Y. Wan, Q. F. Zhao, X. Cao, Y. Ding, Z. L. Wang, H. X. Li and Z. F. Bian, *Nat. Sustain.*, 2021, **4**, 618–626.
25 H. D. She, H. Zhou, L. S. Li, L. Wang, J. W. Huang and Q. Z. Wang, *ACS Sustainable Chem. Eng.*, 2018, **6**, 11939–11948.
26 B. Liu, L. M. Liu, X. F. Lang, H. Y. Wang, X. W. Lou and E. S. Aydil, *Energy Environ. Sci.*, 2014, **7**, 2592–2597.
27 S. L. Candelaria, Y. Y. Shao, W. Zhou, X. L. Li, J. Xiao, J. G. Zhang, Y. Wang, J. Liu, J. H. Li and G. Z. Cao, *Nano Energy*, 2012, **1**, 195–220.
28 T. Zhao, W. Luo, Y. H. Deng, Y. F. Luo, P. C. Xu, Y. Liu, L. J. Wang, Y. Ren and W. Jiang, *Nano Energy*, 2016, **26**, 16–25.
29 H. Wei, E. F. Rodriguez, A. F. Hollenkamp, A. I. Bhatt, D. H. Chen and R. A. Caruso, *Adv. Funct. Mater.*, 2017, **27**, 1703270.
30 W. Zhang, H. L. He, Y. Tian, K. Lan, Q. Liu, C. Y. Wang, Y. Liu, A. Elzatahry, R. C. Che, W. Li and D. Y. Zhao, *Chem. Sci.*, 2019, **10**, 1664–1670.
31 Z. Q. Li, Y. P. Que, L. E. Mo, W. C. Chen, Y. Ding, Y. M. Ma, L. Jiang, L. H. Hu and S. Y. Dai, *ACS Appl. Mater. Interfaces*, 2015, **7**, 10928–10934.
32 X. Q. Liu, J. Iocozzia, Y. Wang, X. Cui, Y. H. Chen, S. Q. Zhao, Z. Li and Z. Q. Lin, *Energy Environ. Sci.*, 2017, **10**, 402–434.
33 O. Ola and M. M. Maroto-Valer, *J. Photochem. Photobiol., C*, 2015, **24**, 16–42.
34 A. Y. Meng, L. Y. Zhang, B. Cheng and J. G. Yu, *Adv. Mater.*, 2019, **31**, 1807660.
35 Z. P. Xing, J. Q. Zhang, J. Y. Cui, J. W. Yin, T. Y. Zhao, J. Y. Kuang, Z. Y. Xiu, N. Wan and W. Zhou, *Appl. Catal., B*, 2018, **225**, 452–467.
36 Z. Xiong, Z. Lei, Y. Z. Li, L. C. Dong, Y. C. Zhao and J. Y. Zhang, *J. Photochem. Photobiol., C*, 2018, **36**, 24–47.
37 M. Humayun, F. Raziq, A. Khan and W. Luo, *Green Chem. Lett. Rev.*, 2018, **11**, 86–102.
38 J. Park, G. H. Moon, K. O. Shin and J. Kim, *Chem. Eng. J.*, 2018, **343**, 689–698.
39 G. Zhang, G. Kim and W. Choi, *Energy Environ. Sci.*, 2014, **7**, 954–966.
40 X. Li and X. J. Lang, *J. Chem. Phys.*, 2020, **152**, 044705.
41 S. S. Lyu, H. M. Hao, X. Li and X. J. Lang, *Chemosphere*, 2021, **262**, 127873.
42 A. L. Yuan, H. Lei, Z. S. Wang and X. P. Dong, *J. Colloid Interface Sci.*, 2020, **560**, 40–49.
43 D. Dissanayake, L. A. Achola, P. Kerns, D. Rathnayake, J. K. He, J. Macharia and S. L. Suib, *Appl. Catal., B*, 2019, **249**, 32–41.
44 D. R. Sun, L. Ye and Z. H. Li, *Appl. Catal., B*, 2015, **164**, 428–432.
45 Z. B. Yu, E. R. Waclawik, Z. J. Wang, X. M. Gu, Y. Yuan and Z. F. Zheng, *J. Mater. Chem. A*, 2017, **5**, 4607–4615.
46 W. H. Sun, Y. G. Xiang, Z. H. Jiang, S. Y. Wang, N. Yang, S. B. Jin, L. H. Sun, H. L. Teng and H. Chen, *Sci. Bull.*, 2022, **67**, 61–70.
47 F. Z. Su, S. C. Mathew, L. Möhlmann, M. Antonietti, X. C. Wang and S. Blechert, *Angew. Chem., Int. Ed.*, 2011, **50**, 657–660.
48 Z. Ma, K. T. Mahmudov, V. A. Aliyeva, A. V. Gurbanov and A. J. L. Pombeiro, *Coord. Chem. Rev.*, 2020, **423**, 213482.
49 H. A. Beejapur, Q. Zhang, K. C. Hu, L. Zhu, J. L. Wang and Z. B. Ye, *ACS Catal.*, 2019, **9**, 2777–2830.
50 H. Xu, Y. F. Zhang and X. J. Lang, *Chin. Chem. Lett.*, 2020, **31**, 1520–1524.
51 X. J. Lang and J. C. Zhao, *Chem.–Asian J.*, 2018, **13**, 599–613.
52 J. Zhou, X. Li, X. M. Ma, W. L. Sheng and X. J. Lang, *Appl. Catal., B*, 2021, **296**, 120368.
53 C. Y. Wu, K. J. Tu, J. P. Deng, Y. S. Lo and C. H. Wu, *Materials*, 2017, **10**, 566.
54 R. Mueller, H. K. Kammler, K. Wegner and S. E. Pratsinis, *Langmuir*, 2003, **19**, 160–165.
55 X. M. Ma and X. J. Lang, *Sustainable Energy Fuels*, 2020, **4**, 1754–1763.
56 M. C. Liu, Y. B. Chen, J. Z. Su, J. W. Shi, X. X. Wang and L. J. Guo, *Nat. Energy*, 2016, **1**, 16151.

